Numerical analysis of quasiperiodic perturbations for the Alfvén wave

Y. Yamakoshi, K. Muto, and Z. Yoshida
Department of Quantum Engineering and Systems Science, The University of Tokyo, Hongo, Tokyo 113, Japan
(Received 16 March 1994)

The Alfvén wave may have a localized eigenfunction when it propagates on a chaotic magnetic field. The Arnold-Beltrami-Childress (ABC) flow is a paradigm of chaotic stream lines and is a simple exact solution to the three-dimensional force-free plasma equilibrium equations. The three-dimensional structure of the magnetic field is represented by sinusoidal quasiperiodic modulation. The short wavelength Alfvén wave equation for the ABC-flow magnetic field has a quasiperiodic potential term, which induces interference among "Bragg-reflected" waves with irregular phases. Then the eigenfunction decays at long distance and a point spectrum occurs. Two different types of short wavelength modes have been numerically analyzed to demonstrate the existence of localized Alfvén wave eigenmodes.

PACS number(s): 52.35.Bj, 02.30.−f, 03.40.Kf, 42.25.−p

I. INTRODUCTION

The magnetohydrodynamic (MHD) spectra in three-dimensional magnetic fields are a challenging subject of perturbation theory for linear operators. It is well known that magnetic field lines have magnetic surfaces if the magnetic field has an ignorable coordinate, i.e., it is two dimensional. A three-dimensional magnetic field does not have surfaces, generally, and field line chaos may occur. Therefore, the spectral structure of the MHD operator is drastically changed in a three-dimensional magnetic field. Among some different branches of MHD spectra, the Alfvén wave is the paradigm of the chaotic perturbation of the magnetic field since the Alfvén wave propagates primarily in the direction parallel to the ambient magnetic field and thus its spectrum is strongly influenced by the field line structure.

In a homogeneous plasma, the dispersion relation of the Alfvén wave is given by a simple relation

$$\omega^2 - \frac{1}{\rho_0 \mu_0}(\boldsymbol{B}\cdot\boldsymbol{k})^2 = 0, \tag{1}$$

where ω is the frequency, $\boldsymbol{k}$ is the wave number vector, ρ_0 is the plasma mass density, and μ_0 is the vacuum permeability. The parallel wave number term $(\boldsymbol{B}\cdot\boldsymbol{k})^2$ comes from the principle part $(\boldsymbol{B}\cdot\nabla)^2$ of the MHD operator, which represents the degenerate characteristics of the Alfvén wave. In a nonuniform magnetic field, $(\boldsymbol{B}\cdot\nabla)^2$ yields continuous spectra [1–4]. Detailed analyses of the Alfvén spectra have been done for various geometries, such as cylindrical geometry [5], axisymmetric toroidal geometry [2,6,7], and nonaxisymmetric toroidal geometry [8–10]. Recently the toroidal effect on the axisymmetric configuration has been attracting much interest because the toroidicity perturbs the continuous spectrum to produce gaps and furthermore to yield point spectra which correspond to the toroidicity-induced shear Alfvén eigenmodes [7,11]. Recent theory [12] studied three-dimensional magnetic fields and predicted point spectra, invoking the analogy of the Alfvén wave in a chaotic magnetic field and the valence electron wave in a quasilattice [13].

In this paper, we present numerical analyses of the spectra of Alfvén waves in a slab geometry with three-dimensional perturbation. The unperturbed magnetic field has magnetic surfaces given by x = const. Three-dimensional perturbation yields chaos of field lines. Our model equation is derived for a chaotic magnetic field represented by Arnold-Beltrami-Childress (ABC) flow. We consider a special class of Beltrami functions which is characterized by

$$\nabla \times \boldsymbol{B} = \lambda \boldsymbol{B}, \tag{2}$$

where λ is a constant. In plasma physics, a magnetic field $\boldsymbol{B}$ that satisfies (2) is force free because $\nabla \times \boldsymbol{B}/\mu_0$ parallels the current density and hence the magnetic stress $(\nabla \times \boldsymbol{B}) \times \boldsymbol{B}/\mu_0$ vanishes in the Beltrami function. The reader is referred to [14] for the mathematical background of the eigenfunctions of the curl. The ABC flow is a simple example of the Beltrami function, which, in Cartesian coordinates reads

$$\boldsymbol{B}(x,y,z) = \begin{pmatrix} A\sin\lambda z + C\cos\lambda y \\ B\sin\lambda x + A\cos\lambda z \\ C\sin\lambda y + B\cos\lambda x \end{pmatrix}, \tag{3}$$

where A, B, C, and λ are real constants. One easily finds that (3) satisfies (2). Field lines are given by $d\boldsymbol{x}/ds = \boldsymbol{B}(\boldsymbol{x})$, where $\boldsymbol{x} = (x,y,z)$. Figure 1 shows Poincaré plots of ABC flows. There exist magnetic surfaces in the whole area when at least one coordinate is ignorable. Magnetic surfaces are destroyed when $\boldsymbol{B}$ is three dimensional, i.e., none of A, B, and C is zero.

The eikonal approximation for short wavelength allows us to reduce the three-dimensional equations into a one-dimensional Schrödinger equation with a quasiperiodic potential [12]. The spectra of quasiperiodic Schrödinger equations have been studied with a smooth potential [15] and with an impulse potential [16]. The method used for spectral analysis of [15] is slightly different from that of

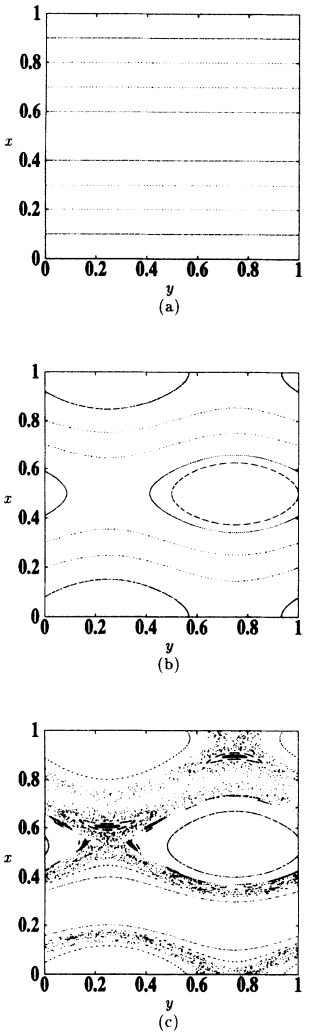

FIG. 1. Poincaré plots of ABC flows with (a) $B = 1$ and $A = C = 0$, (b) $B = 1$, $C = 0.3$, and $A = 0$, and (c) $B = 1$, $C = 0.3$, and $A = 0.2$. Here $\lambda = 2\pi$.

[16]. Here we apply the latter method to the smooth potential. In Sec. II two types of the one-dimensional Alfvén wave equations are discussed. The method for numerical analysis is described in Sec. III. Results are given in Sec. IV.

II. ALFVEN WAVE EQUATION

We consider a slab plasma with a sheared magnetic field

$$\boldsymbol{B}^{(0)}(x) = \begin{pmatrix} 0 \\ B\sin\lambda x \\ B\cos\lambda x \end{pmatrix} \tag{4}$$

and perturb it with

$$\boldsymbol{B}^{(1)}(y,z) = \begin{pmatrix} A\sin\lambda z + C\cos\lambda y \\ A\cos\lambda z \\ C\sin\lambda y \end{pmatrix}, \tag{5}$$

where $|A|,|C| \ll |B|$. The perturbed magnetic field $\boldsymbol{B} = \boldsymbol{B}^{(0)} + \boldsymbol{B}^{(1)}$ is an exact force-free equilibrium; see (3). To simplify calculations, we neglect minor terms and retain the principal terms of the Alfvén wave equation (we assume short wavelengths) and obtain

$$\rho_0 \frac{\partial^2 \psi}{\partial t^2} = \frac{1}{\mu_0}(\boldsymbol{B}\cdot\nabla)^2\psi, \tag{6}$$

where ψ is the vorticity of the deformation in the wave. Substituting the unperturbed magnetic field $\boldsymbol{B}_0$ into (6), we obtain

$$\frac{\partial^2}{\partial t^2}\psi = V_A^2\left(\sin\lambda x\frac{\partial}{\partial y} + \cos\lambda x\frac{\partial}{\partial z}\right)^2\psi, \tag{7}$$

where $V_A = B/\sqrt{\rho_0\mu_0}$ is the Alfvén velocity. Define a local coordinate s in the direction of $\boldsymbol{B}^{(0)}(x)$, i.e., $\nabla s = \boldsymbol{B}^{(0)}/|\boldsymbol{B}^{(0)}|$. Then (7) reads

$$\frac{\partial^2}{\partial t^2}\psi = V_A^2\frac{\partial^2}{\partial s^2}\psi. \tag{8}$$

Fourier transform from t to ω and define $E = \omega^2/V_A^2$ to obtain

$$-\frac{d^2}{ds^2}\psi = E\psi. \tag{9}$$

When the perturbation $\boldsymbol{B}^{(1)}$ is applied, (9) is modified into

$$-\Big[\frac{\partial}{\partial s} + (\epsilon_1\sin\lambda z + \epsilon_2\cos\lambda y)\frac{\partial}{\partial x} + \epsilon_1\cos\lambda z\frac{\partial}{\partial y} + \epsilon_2\sin\lambda y\frac{\partial}{\partial z}\Big]^2\psi + O(\lambda) = E\psi, \tag{10}$$

where $\epsilon_1 = A/B$ and $\epsilon_2 = C/B$ [12]. For some classes of waves, (10) simplifies into ordinary differential equations. First we assume $\partial_x\psi = 0$ at $x = x_0$. Let the angle between the wave vector $\boldsymbol{k}$ and $\boldsymbol{B}^{(0)}$ be $\tan^{-1}\kappa$. Then $|\kappa|$ scales the ratio of perpendicular and parallel wave numbers, i.e., $\kappa = O(k_\perp/k_\parallel)$. We consider waves with large $|\kappa|$ and short wavelength ($|\kappa| \gg |\lambda|$). For fixed κ, (10) reduces into

$$-\frac{d}{ds}[1 + V(s)]^2\frac{d}{ds}\psi = E\psi, \tag{11}$$

where $V(s)$ is an effective potential that is generated by the perturbation

$$V(s) = \nu_1\cos(\lambda\mu_1 s) + \nu_2\sin(\lambda\mu_2 s + \theta_0), \tag{12}$$

where $\nu_1 = \epsilon_1(\sin\lambda x_0 + \kappa\cos\lambda x_0)$, $\nu_2 = \epsilon_2(\cos\lambda x_0 - \kappa\sin\lambda x_0)$, $\mu_1 = \cos\lambda x_0$, $\mu_2 = \sin\lambda x_0$, and x_0 and θ_0 are fixed numbers.

Another class of waves is characterized by long parallel wavelengths (low frequencies). We consider a local mode on a surface $x = x_0$ and write $\psi(x,y,z) = e^{-k_x^2(x-x_0)^2}\psi(y,z)$. We consider short perpendicular wavelengths in the y-z plane and assume

$$|\lambda| \sim |k_\parallel| \ll |k_\perp|, |k_x|, \tag{13}$$

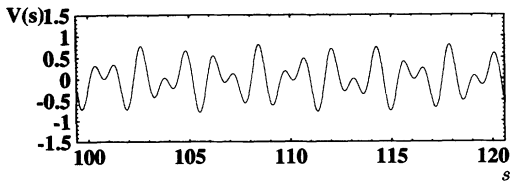

FIG. 2. Quasiperiodic potential for $\nu_1 = \nu_2 = 0.4$, $\sigma = (1+\sqrt{5})/2$, and $\lambda = 2\pi$.

where λ^{-1} is the scale length of the perturbation $\boldsymbol{B}^{(1)}$. Neglecting terms that are of order ϵ_1 and ϵ_2, we obtain

$$-\frac{d^2}{ds^2}\psi + U^2(s)\psi = E\psi, \tag{14}$$

where $U(s)$ is a perturbation potential for the Alfvén wave, which is written as

$$U(s) = a_1 \sin(\lambda\mu_1 s) + a_2 \cos(\lambda\mu_2 s + \theta_0), \tag{15}$$

where $a_1 = k_x\epsilon_1$, $a_2 = k_x\epsilon_2$, and θ_0 is a fixed number. The amplitudes $|a_1|$ and $|a_2|$ of the perturbation may be large (of order λ), when $|k_x|$ is sufficiently large.

When either A or C is zero, or the ratio $\sigma = \mu_2/\mu_1$ is a rational number, $V(s)$ and $U(s)$ are periodic functions. When both A and C are finite and σ is an irrational number, $V(s)$ and $U(s)$ are quasiperiodic (almost periodic) functions. Figure 2 shows $V(s)$ with $\sigma = (1+\sqrt{5})/2$ (the golden ratio). Solutions for the quasiperiodic potential are completely different from those for the periodic potential as discussed below.

III. NUMERICAL ANALYSIS

In this section we present numerical analysis of the one-dimensional Alfén wave equations and show that point spectra occur when the amplitude of the quasiperiodic perturbation becomes large. The corresponding eigenfunctions are spatially localized, resembling Anderson-localized electron wave functions in a quasilattice [9,16,17]. We solve the eigenvalue problems (11) and (14) by three different methods and compare results.

The eigenvalue problems (11) and (14) are written in the form of the first order differential equations

$$\frac{d}{ds}\begin{pmatrix}\psi\\ \dot\psi\end{pmatrix} = \begin{pmatrix}0 & 1\\ -\dfrac{E}{(1+V(s))^2} & -\dfrac{2\dot V(s)}{1+V(s)}\end{pmatrix}\begin{pmatrix}\psi\\ \dot\psi\end{pmatrix} \tag{16}$$

and

$$\frac{d}{ds}\begin{pmatrix}\psi\\ \dot\psi\end{pmatrix} = \begin{pmatrix}0 & 1\\ U^2(s)-E & 0\end{pmatrix}\begin{pmatrix}\psi\\ \dot\psi\end{pmatrix}, \tag{17}$$

respectively, where $\dot f$ indicates the derivative of function f. We solve (16) and (17) with imposing an initial condition $\boldsymbol{\psi}(0) = [\psi(0), \dot\psi(0)]$. To find spectra of equations (11) and (14), we solve (16) and (17) with the parameter E. When E belongs to the point spectra, the corresponding solution $\psi(s)$ decays to zero at long distance. However, it diverges at large s if E is slightly deviated from the spectra. This problem is overcome by treating Eq. (11) or (14) as a boundary-value problem. As for the initial-value method, the shooting method is also effective. The advantage of the initial-value method is that we can easily find whether the eigenvalue E belongs to continuous spectra or point spectra.

Since (16) and (17) are linear equations, Lyapunov exponents are easily calculated by multiplying discrete matrices on (16) or (17); cf. [18]. We use the Lyapunov exponents to observe the long term behavior of $\psi(s)$ and find the point spectra, continuous spectra, and resolvent set.

In solving the eigenvalue problem as an initial value problem, we introduce the phase angle

$$\phi(s) = \tan^{-1}\frac{\sqrt{E}\psi(s)}{\dot\psi(s)} \tag{18}$$

to reduce numerical instability. The evolution of $\phi(s)$ is governed by a nonlinear differential equation; for (16) we obtain

$$\frac{d\phi}{ds} = \sqrt{E}\cos^2\phi + \sqrt{E}\,[1+V(s)]^{-2}\sin^2\phi \tag{19}$$

and for (17)

$$\frac{d\phi}{ds} = \sqrt{E} - \frac{U^2(s)}{\sqrt{E}}\sin^2\phi, \tag{20}$$

where we neglect the first order derivative of $V(s)$ in (16) for short wavelengths. From $\phi(s)$ we can calculate the winding number [9,16,19] defined by

$$w(E) = \lim_{s\to\infty}\frac{\phi(s)}{s}. \tag{21}$$

The winding number corresponds to the final value of angular velocity in the phase space, which is a nondecreasing function of E with plateaus on which $w(E)$ has a constant value $(m\mu_1 + n\mu_2)/2$ $(m, n = 0 \pm 1, \pm 2, \ldots)$. Gaps of spectra (resolvent) correspond to the plateaus of $w(E)$.

A self-adjoint operator has two different groups of spectra, the point spectra and the continuous spectra. The Lyapunov exponent of the phase angle is a strong tool for distinguishing continuous spectra from point spectra. We linearize (19) to obtain

$$\frac{d\delta\phi}{ds} = \sqrt{E}\sin 2\phi\,\left\{[1+V(s)]^{-2} - 1\right\}\delta\phi \tag{22}$$

and (20) to obtain

$$\frac{d\delta\phi}{ds} = -\frac{U^2(s)}{\sqrt{E}}\sin 2\phi\,\delta\phi, \tag{23}$$

where $\delta\phi(s)$ is a small perturbation of $\phi(s)$. The Lyapunov exponent is defined by

TABLE I. The classification of E. ρ, σ_C, and σ_P denote resolvent set, continuous spectrum, and point spectrum, respectively. $\emptyset$ means the empty set.

	$\frac{dw(E)}{dE} = 0$	$\frac{dw(E)}{dE} > 0$
$\Lambda_\phi(E) = 0$	$\emptyset$	σ_C
$\Lambda_\phi(E) < 0$	ρ	σ_P

$$\Lambda_\phi(E) = \lim_{s\to\infty} \frac{\ln[\delta\phi(s)/\delta\phi(0)]}{s}. \tag{24}$$

When $\Lambda_\phi(E) = 0$, the wave function $\psi(s)$ does not diverge or decay to zero at large $|s|$. Hence the corresponding eigenfunction (with infinite energy) belongs to the continuous spectra. When $\Lambda_\phi(E) < 0$, $\psi(s)$ is either unstable or localized. An unstable solution corresponds to the resolvent set, while a localized solution is an eigenfunction corresponding to a point spectrum. The relation between $w(E)$ and $\Lambda_\phi(E)$ is summarized in Table I.

It is usually difficult to obtain eigenfunctions by solving (16) or (17) because of numerical instabilities. We thus appeal to the shooting method, i.e., we impose initial conditions on both end points at long distance and seek E, which makes the logarithmic derivations of the left-hand-side and right-hand-side solutions have the same value at the connection point.

As the third method, we treat (11) and (14) as boundary-value problems. We assume $\psi|_a = \psi|_b = 0$ for large $|b - a|$. We discretize (11) and (14) into

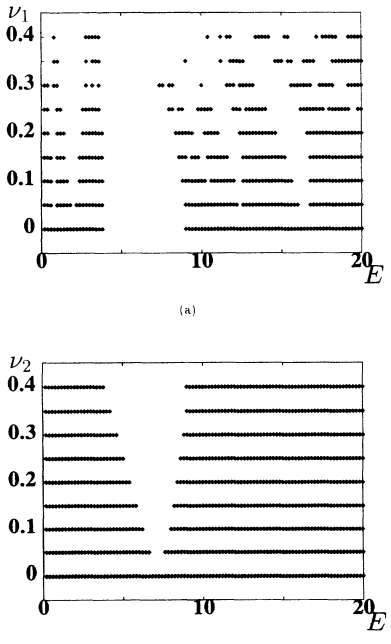

FIG. 3. Overview of continuous spectrum for (a) the quasiperiodic potential ($\nu_2 = 0.4$) and (b) the periodic potential ($\nu_1 = 0$). Here $\lambda = 2\pi$.

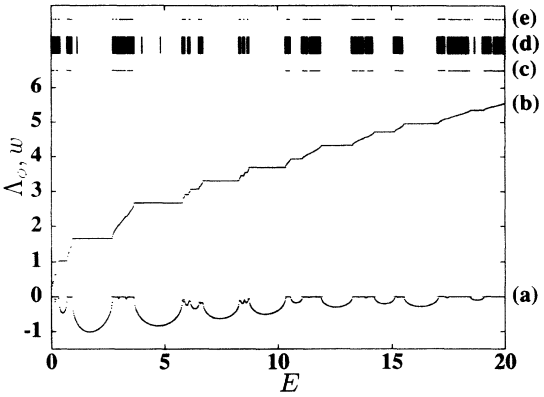

FIG. 4. (a) Lyapunov number Λ_ϕ. (b) Winding number w. (c) Continuous spectra. (d) Spectra obtained from the boundary-value problem. (e) Spectra obtained from the shooting method. Here $\sigma = (1 + \sqrt{5})/2$ and $\lambda = 2\pi$. $E = w^2/V_A^2$ (where V_A is the Alfvén velocity and ω is the frequency. The length is normalized by the scale of the domain.

$$\begin{pmatrix} \alpha_1 & \gamma_1 & & & 0 \\ \beta_1 & \alpha_2 & \gamma_2 & & \\ & \ddots & \ddots & \ddots & \\ & & \ddots & \ddots & \ddots \\ & & & \beta_{N-2} & \alpha_{N-1} & \gamma_{N-1} \\ 0 & & & & \beta_{N-1} & \alpha_N \end{pmatrix} \vec{\psi} \left(\equiv A\vec{\psi}\right) = E\vec{\psi}, \tag{25}$$

$$\vec{\psi} = \begin{pmatrix} \psi_1 \\ \psi_2 \\ \vdots \\ \vdots \\ \psi_{N-1} \\ \psi_N \end{pmatrix},$$

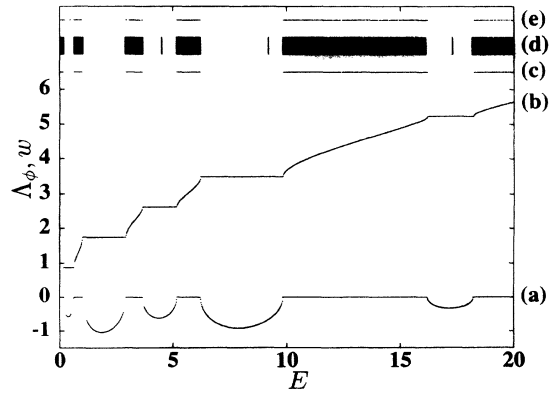

FIG. 5. (a) Lyapunov number Λ_ϕ. (b) Winding number w. (c) Continuous spectra. (d) Spectra obtained from the boundary-value problem. (e) Spectra obtained from the shooting method. Here $\sigma = 3/2$ and $\lambda = 2\pi$.

where, for (11), the diagonal and off-diagonal elements α_j and $\beta_j = \gamma_j$ are given by

$$\alpha_j = \frac{(1+V_{j-\frac{1}{2}})^2}{h^2} + \frac{(1+V_{j+\frac{1}{2}})^2}{h^2}, \quad j = 1,2,\ldots,N, \quad (26)$$

$$\beta_j = \gamma_j = -\frac{(1+V_{j+\frac{1}{2}})^2}{h^2}, \quad j = 1,2,\ldots,N-1, \quad (27)$$

and, for (14),

$$\alpha_j = \frac{2}{h^2} + U_j^2, \quad j = 1,2,\ldots,N, \quad (28)$$

$$\beta_j = \gamma_j = -\frac{1}{h^2}, \quad j = 1,2,\ldots,N-1, \quad (29)$$

where $h = (b-a)/(N+1)$. This formula requires the assumption that the step width h is much smaller than the characteristic length of the potential $V(s)$ or $U(s)$ and that $|b-a|$ is sufficiently large. The matrix of the eigenvalue problem (25) is a symmetric tridiagonal one. We solve the characteristic equation

$$\det(\lambda I - A) = 0, \quad (30)$$

using the method based on Sturm's theorem, and corresponding eigenvectors are computed by inverse iteration method. The computational time is shorter than the previously described initial-value method.

IV. RESULTS

We now present numerical results from two types of reduced equations (11) and (14). An overview of the spectra of (11) is shown in Fig. 3(a). The continuous spectra, which are characterized by $\Lambda_\phi(E) = 0$, are plotted for various ν_1, with $\sigma = (1+\sqrt{5})/2$ and $\nu_2 = 0.4$. One observes that forbidden zones develop as the perturbation amplitude ν_1 increases, and for large ν_1, the bands of continuous spectra become narrow and even disappear. This behavior is compared with the periodic perturbation; see Fig. 3(b). In Fig. 4, the Lyapunov exponent $\Lambda_\phi(E)$, the winding number $w(E)$, and the spectra from the three different methods are plotted for $\nu_1 = \nu_2 = 0.4$ and $\sigma = (1+\sqrt{5})/2$. As discussed in Sec. III, $\Lambda_\phi(E) = 0$ corresponds to the continuous spectrum and $dw(E)/dE = 0$ to the resolvent set. For small or large E, the comple-

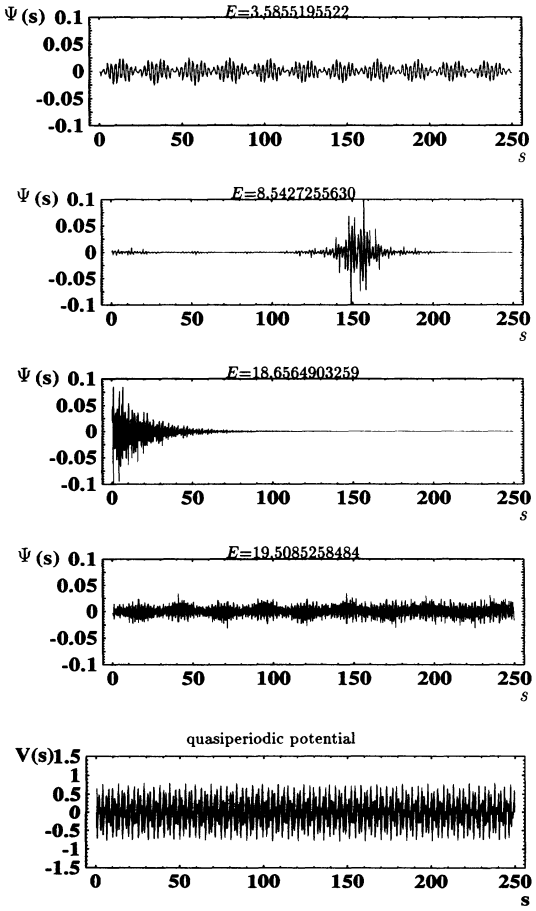

FIG. 6. Eigenfunctions from boundary-value method and the quasiperiodic potential $V(s)$. Here $\nu_1 = \nu_2 = 0.4$ and $\sigma = (1+\sqrt{5})/2$.

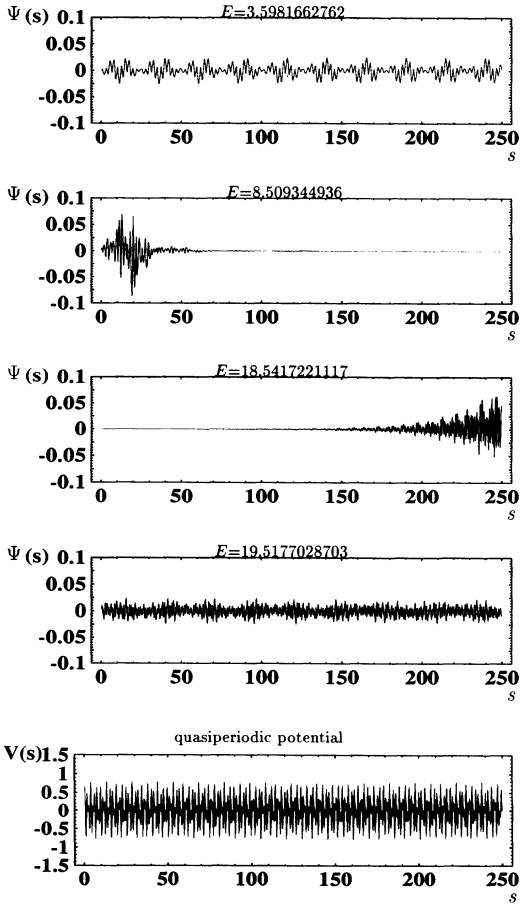

FIG. 7. Eigenfunctions from the shooting method and the quasiperiodic potential $V(s)$.

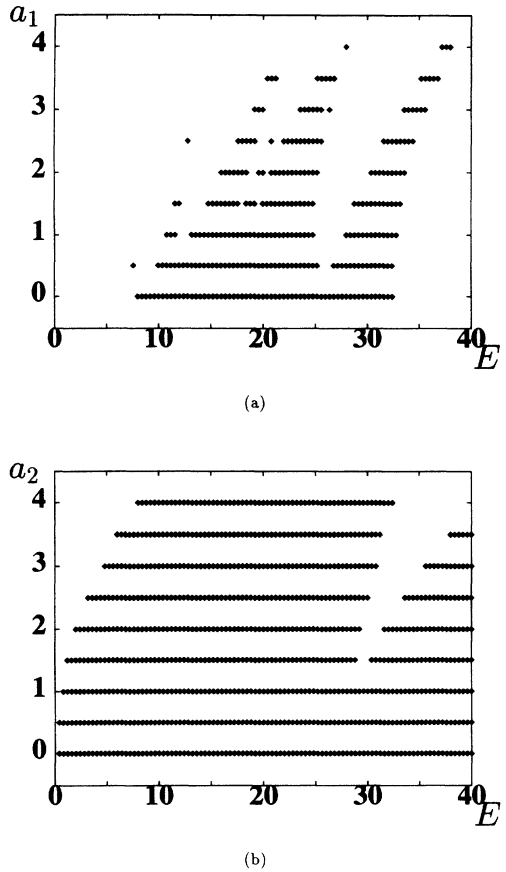

FIG. 8. Overview of continuous spectrum for (a) the quasiperiodic potential ($a_2 = 4.0$) and (b) the periodic potential ($a_1 = 0$). Here $\lambda = 2\pi$.

mentary set of $\{E|\Lambda_\phi(E) = 0\}$ is equal to the set of $\{E|dw(E)/dE = 0\}$. For intermediate E, we find E that satisfies $\Lambda_\phi(E) < 0$ and $dw(E)/dE = 0$, which implies that E is a point spectrum. On the other hand, when the ratio $\sigma = \mu_2/\mu_1$ is a rational number, a point spectrum does not occur; see Fig. 5.

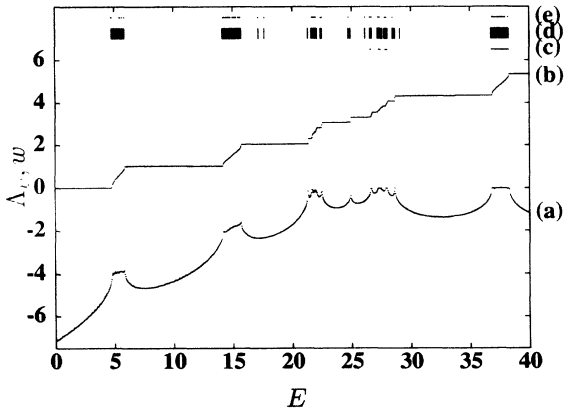

FIG. 9. (a) Lyapunov number Λ_ϕ. (b) Winding number w. (c) Continuous spectra. (d) Spectra obtained from the boundary-value problem. (e) Spectra obtained from the shooting method. Here $\sigma = (1 + \sqrt{5})/2$ and $\lambda = 2\pi$. $E = \omega^2/V_A^2$ (where V_A is the Alfvén velocity and ω is the frequency). The length is normalized by the scale of the domain.

Eigenfunctions were calculated by the boundary-value method and the shooting method (Figs. 6 and 7). Generalized eigenfunctions corresponding to the continuous spectra do not decay at long distance. Eigenfunctions corresponding to point spectra are spatially localized, so that they have finite energies. In addition to them, unstable solutions that grow exponentially at long distance were found in the gap because of numerical errors. Both methods give similar results.

Next, we discuss the second eigenvalue problem (14). Figures 8(a) and 8(b) show overviews of the continuous spectra for the quasiperiodic and periodic perturbations, respectively. In contrast to the first eigenvalue problem (11), a gap appears in the neighborhood of $E = 0$. With a quasiperiodic perturbation, we obtain point spectra with strongly localized eigenfunctions. Figure 9 shows the Lyapunov exponent $\Lambda_\phi(E)$, the winding number $w(E)$, and the spectra calculated from the three different methods. For small E, the magnitude of the Lyapunov exponent is much larger than that of the first case, which implies that the localization is strong. The corresponding eigenfunctions calculated from the boundary-value method are shown in Fig. 10. Figure 11 shows the eigen-

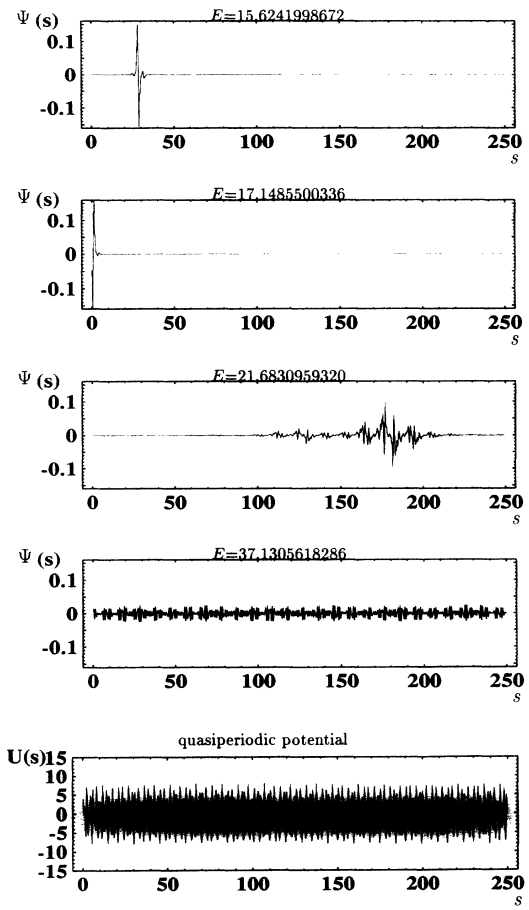

FIG. 10. Eigenfunctions from the boundary-value method and the quasiperiodic potential $U(s)$. Here $a_1 = a_2 = 4.0$ and $\sigma = (1 + \sqrt{5})/2$.

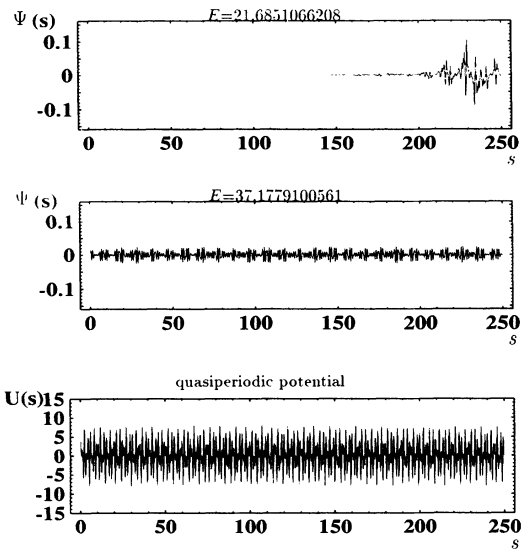

FIG. 11. Eigenfunctions from the shooting method and the quasiperiodic potential $U(s)$. Here $a_1 = a_2 = 4.0$ and $\sigma = (1+\sqrt{5})/2$.

functions calculated from the shooting method. The results from both methods agree well. However, the spectra at $E \sim 15.6$ and $E \sim 17.1$ are not found by the shooting method because the connection of the left and right solutions is difficult to converge when $|\Lambda_\phi(E)|$ is large.

V. SUMMARY

We have analyzed the Alfvén wave equation numerically and demonstrated the existence of localized Alfvén-wave eigenmodes in a chaotic magnetic field. The ABC flow is a paradigm of chaotic stream lines and is a simple exact solution to the three-dimensional force-free plasma equilibrium equations. We have derived equations of Alfvén waves propagating on the ABC flow magnetic field. The three-dimensional structure of the magnetic field is represented by sinusoidal quasiperiodic modulation. We have considered two different branches of short wavelength modes. Both waves satisfy Schödinger-type equations with quasiperiodic potentials, which represent the three-dimensional modulation. The first branch is characterized by short parallel wavelengths (high frequencies). To obtain a localized eigenmode with a high frequency, we need a relatively large perturbation, which resembles the tight-binding system [12]. The second branch assumes large $k_\perp$ and long parallel wavelength. A large $k_\perp$ enhances the effect of perturbation; see (12) and (15). In the limit of $|k_\perp| \to +\infty$, the characteristic equation (the eikonal) of the Alfvén wave equation, which is identical to the magnetic field line, gives the orbit of an Alfvén wave beam. A narrow beam with a chaotic orbit (i.e., the magnetic field line) may not have a long scale structure, so that the field line chaos yields a localized eigenmode.

ACKNOWLEDGMENTS

The authors are grateful to Professor T. Hatori, Dr. N. Nakajima, Professor N. Inoue, and Dr. Y. Ogawa for their discussions and comments.

[1] J. Tataronis and W. Grossman, Z. Phys. **14**, 203 (1973).
[2] J. P. Goedbloed, Phys. Fluids **18**, 1258 (1975).
[3] E. Hameiri, Commun. Pure Appl. Math. **38**, 43 (1985).
[4] A. Hasegawa and C. Uberoi, *The Alfvén Wave*, DOE Critical Review Series DOE/TIC-11197 (Technical Information Center, U.S. Department of Energy, Springfield, VA, 1982).
[5] K. Appert, R. Gruber, and J. Vaclavik, Phys. Fluids **17**, 1471 (1974).
[6] C. E. Kieras and J. A. Tataronis, Phys. Fluids **25**, 1228 (1982).
[7] C. Z. Cheng and M. S. Chance, Phys. Fluids **29**, 3695 (1986).
[8] M. P. Bernardin and J. A. Tataronis, Phys. Fluids **27**, 133 (1984).
[9] A. Salat, Plasma Phys. Controlled Fusion **34**, 1339 (1991).
[10] N. Nakajima, C. Z. Chang, and M. Okamoto, Phys. Fluids B **4**, 1115 (1992).
[11] J. W. Van Dam, G. Y. Fu, and C. Z. Cheng, Fusion Technol. **18**, 461 (1990).
[12] Z. Yoshida, Phys. Rev. Lett. **68**, 3168 (1992).
[13] D. A. D'Ippolioto and J. P. Goedbloed, Plasma Phys. **22**, 1091 (1980).
[14] Z. Yoshida and Y. Giga, Math. Z. **204**, 235 (1990); Z. Yoshida, J. Math. Phys. **33**, 1252 (1992).
[15] A. Bondeson, E. Ott, and T. M. Antonsen, Jr., Phys. Rev. Lett. **55**, 2103 (1985).
[16] A. Salat, Phys. Rev. A **45**, 1116 (1991).
[17] B. Simon, Adv. Appl. Math. **3**, 463 (1980).
[18] A. Crisanti, G. Paladin, and A. Vulpiani, *Products of Random Matrices* (Springer-Verlag, Berlin, 1993).
[19] R. Johnson and J. Moser, Commun. Math. Phys. **84**, 403 (1982).